Journal of Power Sources 244 (2013) 328–335

Contents lists available at SciVerse ScienceDirect

Journal of Power Sources

journal homepage: www.elsevier.com/locate/jpowsour

Urchin-like α-MnO_2 decorated with Au and Pd as a bi-functional catalyst for rechargeable lithium–oxygen batteries

Kyu-Nam Jung [a,1], Ahmer Riaz [a,b,1], Seung-Bok Lee [a], Tak-Hyoung Lim [a], Seok-Joo Park [a], Rak-Hyun Song [a], Sukeun Yoon [a], Kyung-Hee Shin [a], Jong-Won Lee [a,b,*]

[a] New and Renewable Energy Research Division, Korea Institute of Energy Research, 152 Gajeong-ro, Yuseong-gu, Daejeon 305-343, Republic of Korea
[b] Department of Advanced Energy Technology, University of Science and Technology, 217 Gajeong-ro, Yuseong-gu, Daejeon 305-350, Republic of Korea

HIGHLIGHTS

- Nanostructured composite catalysts for rechargeable lithium–oxygen batteries.
- Urchin-like α-MnO_2 decorated with Au and Pd nanoparticles.
- The catalysts show high bi-functional activity for oxygen reduction and evolution.
- The catalysts reduce discharge–charge overpotentials of a hybrid Li–O_2 battery.

ARTICLE INFO

Article history:
Received 17 October 2012
Received in revised form
11 December 2012
Accepted 3 January 2013
Available online 12 January 2013

Keywords:
Lithium–oxygen battery
Cathode
Manganese oxides
Metal decoration
Oxygen reduction
Oxygen evolution

ABSTRACT

Rechargeable lithium–oxygen batteries have attracted considerable attention due to their high energy density. The critical challenges that limit the practical use of this technology include sluggish kinetics of the electrochemical oxygen reactions on the cathode during discharging and charging. Here, urchin-like α-MnO_2 materials decorated with Au and Pd nanoparticles are developed for use as a cathode catalyst for rechargeable Li–O_2 batteries with hybrid electrolytes. Au and Pd particles as large as 3–8 nm are uniformly dispersed on the vertically aligned nanorods of α-MnO_2. The Au/α-MnO_2 and Pd/α-MnO_2 catalysts show excellent bi-functional activity for both oxygen reduction and evolution. A rechargeable Li–O_2 battery with a hybrid electrolyte is constructed using the nanostructured composite catalysts. Charging and discharging experiments of the batteries indicate that the metal-decorated, urchin-like α-MnO_2 can be used as an efficient bi-functional catalyst for rechargeable hybrid Li–O_2 batteries.

1. Introduction

Rechargeable metal-oxygen batteries have received significant attention in recent years, due to an increasing need for high-energy density storage for electric vehicle applications [1]. Metal-oxygen batteries generate electricity through an oxidation reaction of a metal anode and a reduction reaction of oxygen on a cathode. Among various cell chemistries, in principle, lithium–oxygen batteries offer the highest energy density due to the high capacity of the Li anode and high operating potentials of the Li–O_2 couple [2,3]. The concept of the Li–O_2 battery was first introduced by researchers at Lockheed who used an aqueous alkaline electrolyte [4], but the development was abandoned in the late 1980s due to the undesirable reaction of Li with water. Then, Abraham and Jiang [5] demonstrated an electrically rechargeable Li–O_2 battery with a non-aqueous electrolyte. Following this work, extensive study on non-aqueous Li–O_2 batteries has been conducted to improve energy density and cyclability [6–9]. However, there are still critical problems associated with non-aqueous batteries: for example, (*i*) clogging of oxygen cathodes by insoluble discharge products (*e.g.*, Li_2O_2) and (*ii*) decomposition of organic electrolytes upon cycling due to attacks by reduced O_2 species [3,9–11].

Recently, Zhou and co-workers [12–14] proposed a rechargeable Li–O_2 battery with a "hybrid" electrolyte that could circumvent the problems of both batteries using aqueous and non-aqueous

* Corresponding author. New and Renewable Energy Research Division, Korea Institute of Energy Research, 152 Gajeong-ro, Yuseong-gu, Daejeon 305-343, Republic of Korea. Tel.: +82 42 860 3025; fax: +82 42 860 3297.
E-mail address: jjong277@kier.re.kr (J.-W. Lee).
[1] Equally contributed.

0378-7753/$ – see front matter © 2013 Elsevier B.V. All rights reserved.
http://dx.doi.org/10.1016/j.jpowsour.2013.01.028

electrolytes. The hybrid electrolyte consists of a non-aqueous electrolyte on the Li anode side and an aqueous electrolyte on the cathode side, and the two electrolytes are separated by a water-stable, Li^+-conducting solid membrane (*e.g.*, $Li_{1+x+y}Ti_{2-x}Al_xP_{3-y}Si_yO_{12}$, LTAP) (Fig. 1). Discharging and charging processes of a hybrid Li–O_2 battery involve the oxygen reduction reaction (ORR) and the oxygen evolution reaction (OER) in an aqueous electrolyte, respectively. Experimental studies [14–16] have indicated that hybrid Li–O_2 batteries suffer from sluggish kinetics of ORR and OER on the cathode.

Until now, Pt and its alloys have been considered the best bi-functional catalysts for ORR and OER in metal-oxygen batteries and fuel cells. However, Pt remains an expensive metal of low abundance. Therefore, much of the focus has moved toward cheap and abundant catalytic materials based on transition metal oxides. Manganese oxides (MnO_x) have been widely studied as an alternative to Pt-based catalysts because of their many advantages, such as abundance, low cost, environmental friendliness, and acceptable activity [17–20]. Among various MnO_x polymorphs, α-MnO_2 is believed to be a promising bi-functional catalyst for ORR and OER [19–21]. Early reports [19,21] suggested that higher activity of α-MnO_2 is attributed to the 2 × 2 tunnel frame structure and large number of defects and –OH groups that promote O_2 adsorption and dissociation of the O–O bond. Nevertheless, it is evident that the bi-functional activity of α-MnO_2 still falls below those of Pt-based catalysts.

In an attempt to develop a cost-effective bi-functional catalyst with high activity for rechargeable hybrid Li–O_2 batteries, here, we report nanostructured composite catalysts, *i.e.*, urchin-like α-MnO_2 decorated with a small amount of Au or Pd. An urchin-like MnO_2 particle has numerous nanorods that are vertically grown on a spherical core and, thus, it may provide a large surface area and excellent accessibility of active species during ORR and OER. In this work, Au and Pd that have a lower cost than Pt are noble metals of our interest, since they have been reported to possess relatively high ORR activity in alkaline media [22–24]. An urchin-like α-MnO_2 material was successfully synthesized and decorated with 2 wt.% Au or Pd nanoparticles. The bi-functional catalytic activity of Au/α-MnO_2 and Pd/α-MnO_2 was investigated with a rotating-disk electrode (RDE) technique. Furthermore, hybrid Li–O_2 batteries were constructed and tested using the synthesized composite catalysts.

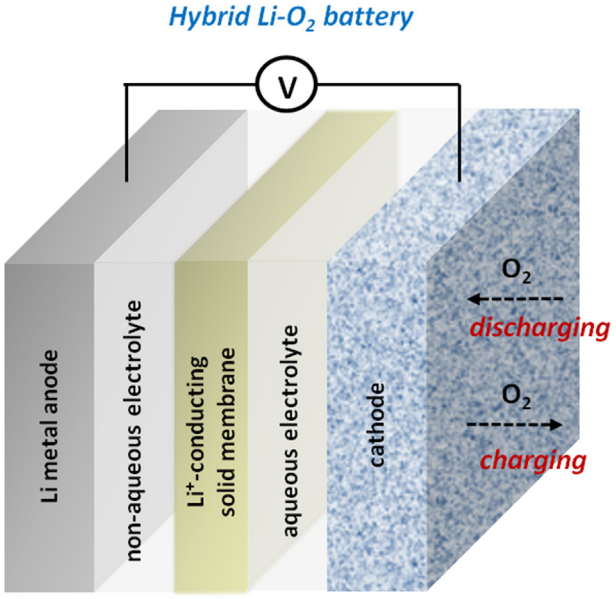

Fig. 1. Schematic diagram of a hybrid Li–O_2 cell.

2. Experimental

2.1. Synthesis of urchin-like α-MnO_2

All of the chemicals used were of analytical grade, purchased from Sigma Aldrich and used without any subsequent treatment. An urchin-like α-MnO_2 material was synthesized *via* chemical oxidation of $MnSO_4$ in the presence of $AgNO_3$ without subsequent heat-treatment. In a typical procedure, 6 mL of concentrated H_2SO_4 was mixed with 300 mL of deionized water and heated to either 30 or 70 °C. 6 mmol of $(NH_4)_2S_2O_8$ and 6 mmol of $MnSO_4$ were dissolved into the mixed solution and, then, 3 mL of $AgNO_3$ solution (0.059 M) was added. Here, Ag^+ was used as a catalyst to facilitate the formation of urchin-like nanostructures. The resulting solution was refluxed for 48 h, and the black-colored precipitates were collected by filtration, washed with alcohol and water, and dried under vacuum overnight at 120 °C.

2.2. Synthesis of Au/α-MnO_2 and Pd/α-MnO_2

Nanosized Au or Pd particles were loaded on the urchin-like α-MnO_2 by using ascorbic acid ($C_6H_8O_6$) as a reducing agent. Typically, 1.44 mmol of sodium citrate ($HOC(COONa)(CH_2COOH)_2$) and 1.44 mmol of poly vinyl propylene (PVP) were dissolved into 200 mL of water and heated to 80 °C. For the preparation of Au/α-MnO_2, 1.24 mL of $HAuCl_4$ solution (0.06 M) was added to the reaction mixture and, then, 11.75 mL of ascorbic acid solution (0.06 M) was added drop wise. The molar ratios of [sodium citrate:gold chloride] and [PVP:gold chloride] were maintained at 20:1 as well. The solution was kept for 1 h under stirring conditions. After that, 0.6 g of α-MnO_2 dispersed in 100 mL of deionized water was added to the reaction mixture and refluxed at 80 °C for 4 h. The Au loading on α-MnO_2 was 2 wt.%. The resulting powder was filtered, washed with alcohol and water, and dried under vacuum at 120 °C for 12 h. N_2 gas was purged into the reaction mixture throughout the experiment. Pd/α-MnO_2 was prepared under the same conditions except K_2PdCl_6 was used as a Pd precursor.

2.3. Materials characterization

In order to identify the crystal structures of the synthesized catalysts, X-ray diffraction (XRD) patterns were recorded with an automated Rigaku diffractometer (2500 D/MAX, Rigaku) using a Cu K_α (λ = 1.54056 Å) radiation. The measurements were conducted over the scanning angle range of 10–90° at a scan rate of 5° min^{-1}. The morphology of the synthesized catalysts was examined with scanning electron microscopy (SEM, Hitach X-4900) and transmission electron microscopy (TEM, Hitachi H9000). The Brunauer–Emmett–Teller (BET) surface area was determined from N_2 sorption isotherms by using a BEL-SORP mini system.

2.4. Electrochemical measurements

RDE experiments were performed in a three-electrode electrochemical cell using a potentiostat (CH Instrument) at room temperature. An RDE with a glassy carbon substrate (diameter = 3 mm) was used as the working electrode. The catalyst ink was prepared by blending the catalyst (50 wt.%) and the conductive carbon (Ketjen Black, 50 wt.%) with the distilled water in an ultrasonic bath. The suspension was deposited onto the glassy carbon electrode that was polished with Al_2O_3 powders. The weight of the electrode loaded on the RDE was 20 μg. After drying, 5 μL of Nafion solution (5 wt.%) was coated onto the catalyst layer to ensure the adhesion on the glassy carbon substrate. The electrolyte was 0.1 M KOH solution. A Pt wire and an Ag/AgCl electrode were used as the

counter and reference electrodes, respectively. All potentials in this work were referred to a reversible hydrogen electrode (RHE). O_2 gas was purged throughout the RDE experiments to make the electrolyte saturated with oxygen, and the linear sweep voltammogram was recorded at a rate of 10 mV s^{-1} by scanning the electrode potential from 1.1 to 0.4 V *vs.* RHE for ORR and from 1.0 to 2.0 V *vs.* RHE for OER.

To prepare the cathode for a hybrid Li–O_2 battery, a composite powder of the catalyst and the conductive carbon (Ketjen Black) was mixed with poly(tetrafluoroethylene) (PTFE) binder in ethanol. The cathode consisted of 30 wt.% catalyst, 65 wt.% carbon black and 5 wt.% binder. Then, the mixture was pressed with a twin roller and dried under vacuum at 60 °C for 24 h. Finally, the cathode was prepared by pressing the composite sheet (thickness = *ca.* 200 μm) onto a nickel mesh current collector. The electrode loading was 30 mg cm^{-2}. The Li–O_2 cell with a hybrid electrolyte consists of a lithium foil anode, a non-aqueous electrolyte, a solid membrane, an aqueous electrolyte, and a cathode. The anode compartment was first assembled by stacking (*i*) a copper mesh current collector, (*ii*) a lithium foil, (*iii*) a polypropylene separator (Celgard® 2400) impregnated with 1 M lithium bis(trifluoromethanesulfonyl)imide (LiTFSI) in tetraethylene glycol dimethyl ether (TEGDME), and (*iv*) an $Li_{1+x+y}Ti_{2-x}Al_xP_{3-y}Si_yO_{12}$ (LTAP) solid membrane (OHARA Inc.). It was sealed using an Al pouch, leaving a square window of 2.5 × 2.5 cm^2. The anode was fabricated in a glove box filled with purified Ar gas. After the sealed anode was taken out of the glove box, a mixed aqueous electrolyte of 1 M $LiNO_3$ and 0.5 M LiOH was poured on the top of the LTAP solid membrane and, then, the cathode was placed on the aqueous electrolyte. The hybrid Li–O_2 battery assembled in this work is schematically illustrated in Fig. 2. The electrochemical performance of the Li–O_2 battery was evaluated by a galvanostatic charge–discharge method with a Maccor series 4000.

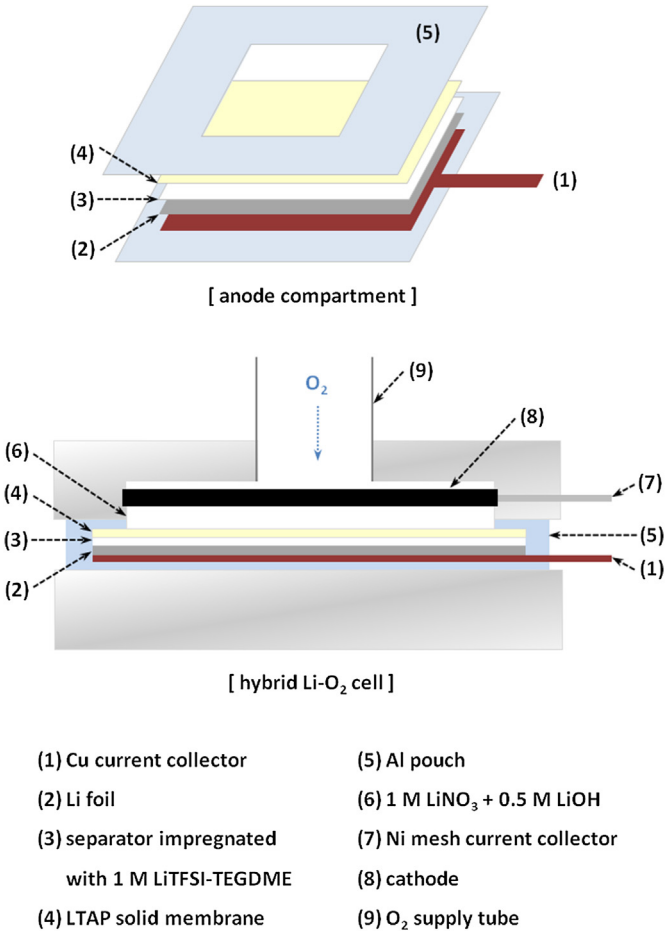

Fig. 2. Schematic diagram of the hybrid Li–O_2 cell used for electrochemical tests.

3. Results and discussion

Fig. 3(a) shows the powder XRD patterns of the MnO_2 specimens prepared at 30 and 70 °C. All of the diffraction peaks can be indexed to the tetragonal cryptomelane phase of α-MnO_2. The diffraction peaks of α-MnO_2 became sharper at 70 °C, indicating that the crystallinity improved with an increase of the synthesis temperature. The SEM micrographs of α-MnO_2 prepared at 30 and 70 °C are presented in Fig. 3(b). The MnO_2 particles have an urchin-like morphology with nanorods vertically grown on a spherical core. As shown in Fig. 3(b), the lengths of the nanorods increase with an increasing temperature from 30 to 70 °C, which indicates that the one-dimensional growth habit of α-MnO_2 is enhanced at higher temperatures. In fact, the α-MnO_2 material prepared at 70 °C exhibited a larger BET surface area (78.0 m^2 g^{-1}) compared to that synthesized at 30 °C (47.7 m^2 g^{-1}) and, hence, the former was used as a support for the loading of Au or Pd nanoparticles.

Fig. 4(a) presents the powder XRD patterns of the Au/α-MnO_2 and Pd/α-MnO_2 catalysts. Both of the XRD patterns show the characteristic peaks corresponding to α-MnO_2, which confirms that the crystal structure of α-MnO_2 is preserved without being destroyed during metal decoration. In addition, the low-magnification TEM image in Fig. 4(b) demonstrates that the loading process of Au does not cause any changes in the urchin-like morphology of α-MnO_2. The TEM images with higher magnifications in Fig. 4(c)–(e) show that Au and Pd particles as large as 3–8 nm are uniformly dispersed on the surface of α-MnO_2 nanorods (40–50 nm in diameter).

The bi-functional catalytic activity of pristine α-MnO_2, Au/α-MnO_2 and Pd/α-MnO_2 for ORR and OER in an aqueous electrolyte was determined by RDE experiments. Fig. 5(a) illustrates the typical polarization curves for ORR in a 0.1 M KOH solution. The catalytic activity increases in the order of pristine α-MnO_2 < Pd/α-MnO_2 < Au/α-MnO_2, as evidenced by (*i*) higher onset potentials for ORR, and (*ii*) higher half-wave potentials (*i.e.*, higher current in the mixed kinetic-diffusion controlled region), and (*iii*) larger limiting currents. In particular, the α-MnO_2 catalyst decorated with 2 wt.% Au nanoparticles shows an onset potential for ORR as high as 0.96 V *vs.* RHE, which is comparable to those of Pt-based catalysts reported in previous studies [16,23,25].

In general, oxygen reduction in an alkaline electrolyte proceeds by two pathways as follows [22]:

$$\begin{array}{c} \overset{1}{\overbrace{\uparrow \qquad \downarrow}} \\ O_{2,b} \rightarrow O_{2,a} \xrightarrow{2} HO_{2,a}^{-} \xrightarrow{3} OH^{-} \\ \downarrow 4 \\ HO_2^{-} \end{array} \qquad (1)$$

where subscripts *a* and *b* denote the species adsorbed on the electrode surface and in the bulk, respectively. O_2 may be directly reduced to OH^- through four-electron transfer (Reaction 1). In parallel, O_2 may be reduced to HO_2^- *via* two-electron transfer (Reaction 2), followed by either reduction of HO_2^- to OH^- (Reaction 3) or transport of the adsorbed HO_2^- to the bulk solution (Reaction 4). According to Eq. (1), the four-electron transfer reaction is more oxygen-efficient for current production than the two-electron transfer reaction. Thus, the number of electrons (*n*) exchanged

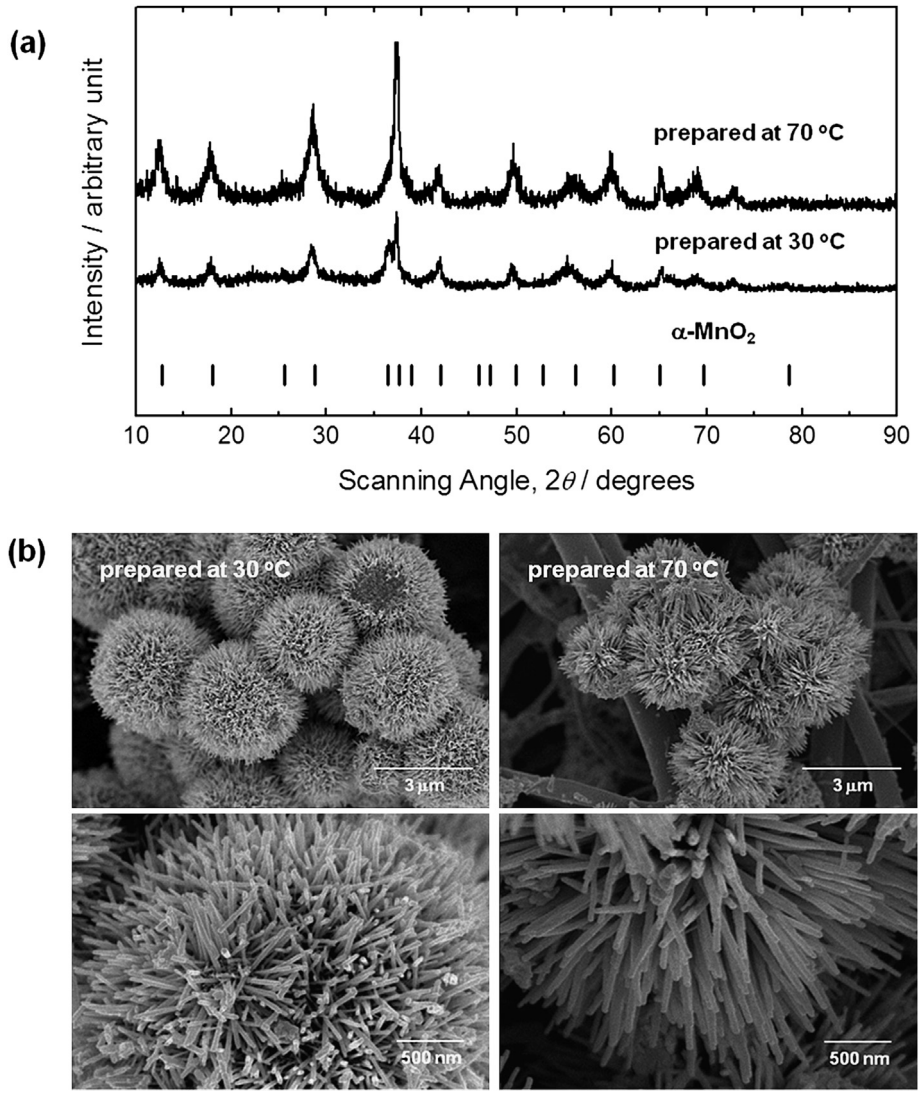

Fig. 3. (a) Powder XRD patterns and (b) SEM images of the MnO_2 materials synthesized at 30 and 70 °C.

during ORR is an important parameter for characterizing the catalyst performance.

The polarization curves obtained at various rotation rates were used to construct the Koutecky–Levich (K–L) plots based on Eq. (2) [26] and then analyzed to determine the value of n:

$$\frac{1}{I} = \frac{1}{I_k} + \frac{1}{I_d} = \frac{1}{nFAkC_{O_2}} + \frac{1}{0.62nFAD_{O_2}^{2/3}\omega^{1/2}\nu^{-1/6}C_{O_2}} \quad (2)$$

where I is the measured current, I_k the kinetic current in the absence of diffusion limitation, I_d the diffusion-limited current, F the Faraday constant, A the geometric surface area, k the rate constant, C_{O_2} the bulk concentration of oxygen in 0.1 M KOH, D_{O_2} the diffusion coefficient of oxygen in the bulk solution, ω the rotation rate, and ν represents the kinetic viscosity of the electrolyte. Fig. 5(b)–(d) show the typical K–L plots for pristine α-MnO_2, Au/α-MnO_2 and Pd/α-MnO_2, respectively. The current values measured at 0.6 V *vs.* RHE were used to make the K–L plots. A linear relationship between I^{-1} and $\omega^{-1/2}$ is clearly observed as predicted from Eq. (2). The values of n calculated from Eq. (2) are 3.3, 3.2 and 3.8 for pristine α-MnO_2, Au/α-MnO_2 and Pd/α-MnO_2, respectively.

The detailed reaction pathway for ORR on MnO_2 could be described in terms of the adsorption sites of oxygen molecules [19]: (*i*) oxygen molecule may be adsorbed on two neighboring MnOOH sites with a breakage of O=O bond (four-electron transfer) and/or (*ii*) the oxygen molecule is likely to be adsorbed on a single Mn site without breakage of the O=O bond (two-electron transfer). Therefore, the catalytic activity of MnO_2 for ORR strongly depends on the morphological properties as well as the crystallographic structure [19,27]. In the present work, the result of $n = 3.3$ for the pristine α-MnO_2 catalyst indicates that ORR proceeds simultaneously *via* the two- and four-electron transfer reactions. The value of n obtained for the urchin-like α-MnO_2 is quite consistent with those for α-MnO_2 with one-dimensional nanostructures (*e.g.*, nanowire) reported in the previous paper [19].

It should be noted that the n value for the Au/α-MnO_2 catalyst is similar to that of pristine α-MnO_2. This means that the Au decoration has no significant influence on the ORR mechanism. It is known that the mechanism of oxygen reduction on an Au metal is strongly dependent on the size of Au particles. For example, Tang et al. [28] showed that 3 nm particles catalyzed ORR *via* four-electron transfer, whereas the two-electron transfer mechanism

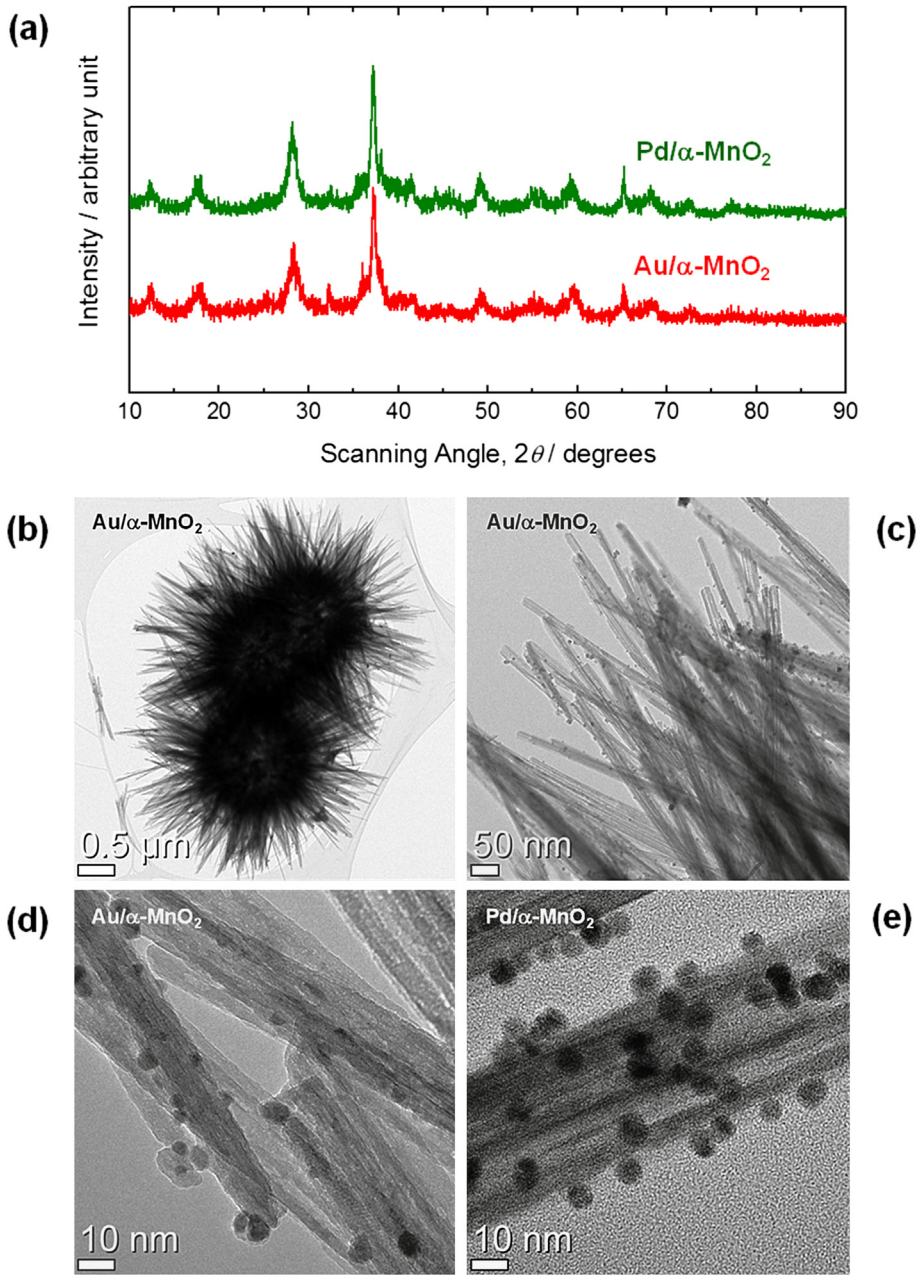

Fig. 4. (a) Powder XRD patterns and (b)–(e) TEM images of the Au/α-MnO_2 and Pd/α-MnO_2 catalysts.

is operative on 7 nm particles. They speculated that the high density of low-coordination sites on the 3 nm particles may promote the activation of HO_2^- species, thereby facilitating the four-electron transfer reactions. Given that in this work, Au particles loaded on α-MnO_2 has some size distribution between 3 and 8 nm, the combined two- and four-electron pathways are operative on Au nanoparticles and, hence, the *n* value remains almost unchanged even after Au decoration. On the other hand, the *n* value increased from 3.3 to 3.8 when Pd nanoparticles were loaded on α-MnO_2. This could be explained by the fact that Pd nanoparticles mainly catalyze four-electron reaction, as experimentally verified in the previous studies [23,29].

To evaluate the ability to catalyze OER, we measured the polarization curves on the RDE during the anodic potential scan up to 2.0 V *vs.* RHE as shown in Fig. 6. The Au/α-MnO_2 catalyst exhibits higher OER currents when compared with pristine α-MnO_2 and Pd/α-MnO_2. The RDE results of Figs. 5 and 6 may be summarized as follows: (*i*) the decoration of α-MnO_2 with Au and Pd nanoparticles results in an enhanced catalytic activity for both ORR and OER, (*ii*) the Au decoration is more effective for promoting ORR and OER than the Pd decoration, and (*iii*) the Pd decoration facilitates the four-electron transfer reaction, whereas the Au decoration has no significant effect on the ORR mechanism.

With the ORR and OER activity of the metal-decorated MnO_2 catalysts proven in the RDE experiments, the hybrid Li–O_2 battery was constructed using the developed composite catalysts, and the discharge–charge performance of the batteries was evaluated. Fig. 7(a) presents the galvanostatic discharge and charge profiles of the hybrid Li–O_2 batteries measured at a current density of

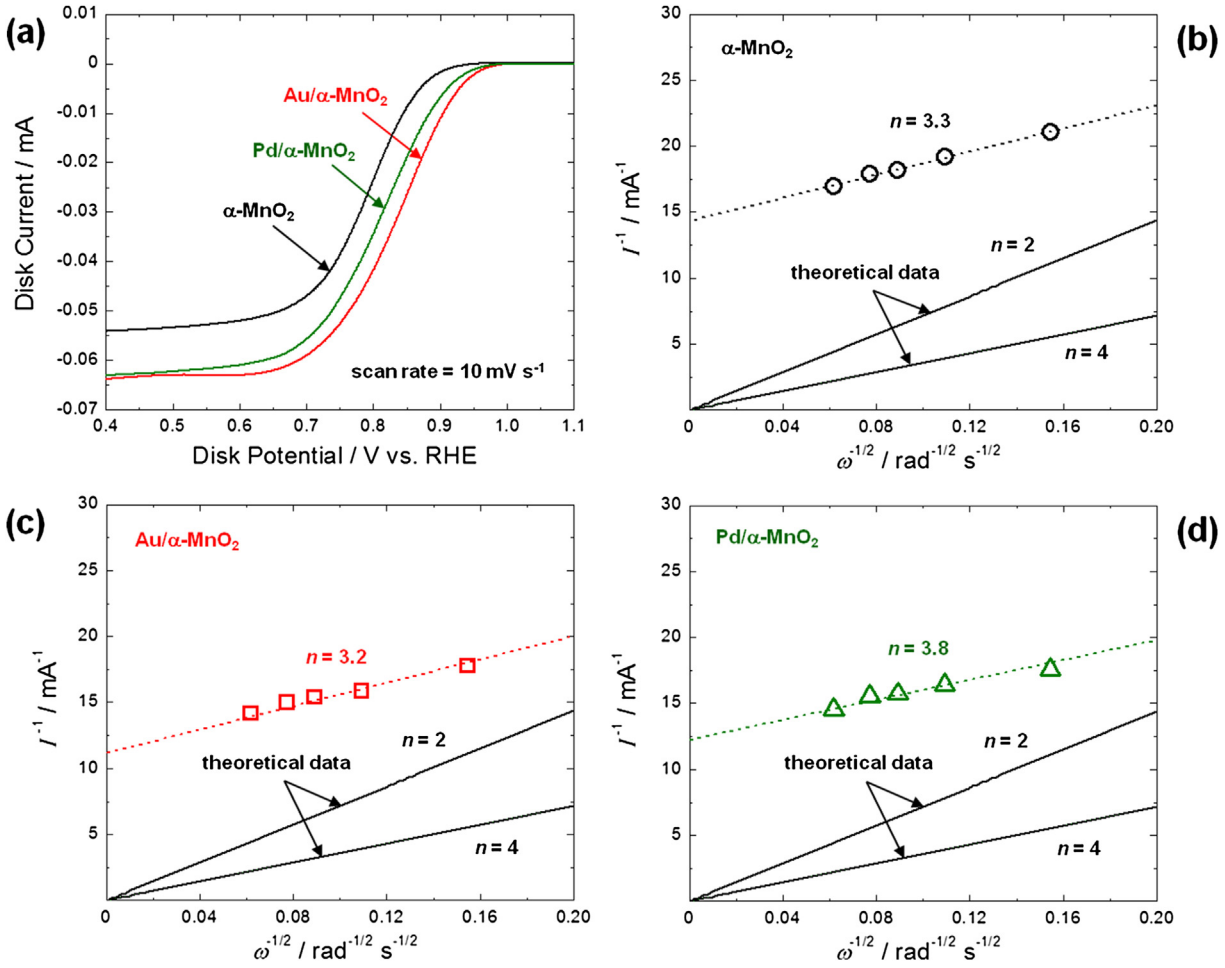

Fig. 5. (a) ORR polarization curves on the RDE at 800 rpm in 0.1 M KOH for the pristine α-MnO_2, Au/α-MnO_2 and Pd/α-MnO_2 catalysts. Koutecky–Levich plots at 0.6 V *vs.* RHE measured on (b) α-MnO_2, (c) Au/α-MnO_2 and (d) Pd/α-MnO_2.

0.6 mA cm^{-2}. On discharging (charging), the cell voltage monotonously decreases (increases) and then reaches a steady-state value. The overpotentials for discharge and charge are believed to be determined by the kinetics of oxygen reactions at the cathode as well as the internal resistances of the Li anode and LTAP solid membrane. As shown in Fig. 7(a), the performance of the hybrid Li–O_2 battery is strongly dependent on the cathode catalyst. The discharge voltages at the steady-state were determined to be 2.78 V, 2.85 V and 2.89 V for pristine α-MnO_2, Pd/α-MnO_2 and Au/α-MnO_2, respectively. Here, the steady-state charge voltage increases in the order of Au/α-MnO_2 (3.68 V) < Pd/α-MnO_2 (3.75 V) < pristine α-MnO_2 (3.77 V). It is obvious that the reduced discharge–charge overpotentials of the hybrid Li–O_2 battery assembled with the Au/α-MnO_2 catalyst resulted from higher bi-functional activity, as revealed by the RDE measurements.

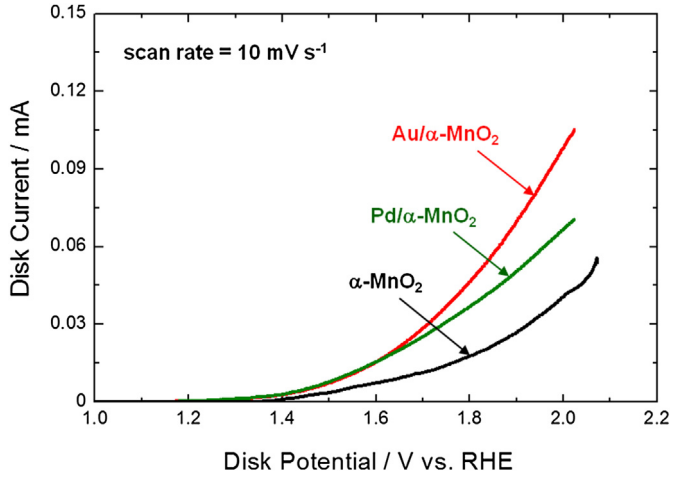

Fig. 6. OER polarization curves on the RDE at 1200 rpm in 0.1 M KOH for the pristine α-MnO_2, Au/α-MnO_2 and Pd/α-MnO_2 catalysts.

Fig. 7(b) gives the plots of the steady-state cell voltage against the applied current measured during discharging and charging. It can be seen that the Au/α-MnO_2 catalyst reduces overpotentials over the entire current ranges and, hence, can be used as an efficient catalyst for the bi-functional cathode in rechargeable hybrid Li–O_2 batteries. The discharge–charge curves during consecutive cycles are also shown in Fig. 7(c). The hybrid Li–O_2 battery assembled with the Au/α-MnO_2 catalyst exhibits more stable cycling performance compared to the battery with Pd/α-MnO_2. It is seen that the discharge–charge overpotentials gradually increase with cycle number. The possible origins for the increased overpotentials include (*i*) the dissolution of catalysts, (*ii*) the oxidation of carbon materials at high potentials, (*iii*) the growth of lithium dendrites on the anode and (*iv*) the degradation of the LTAP solid

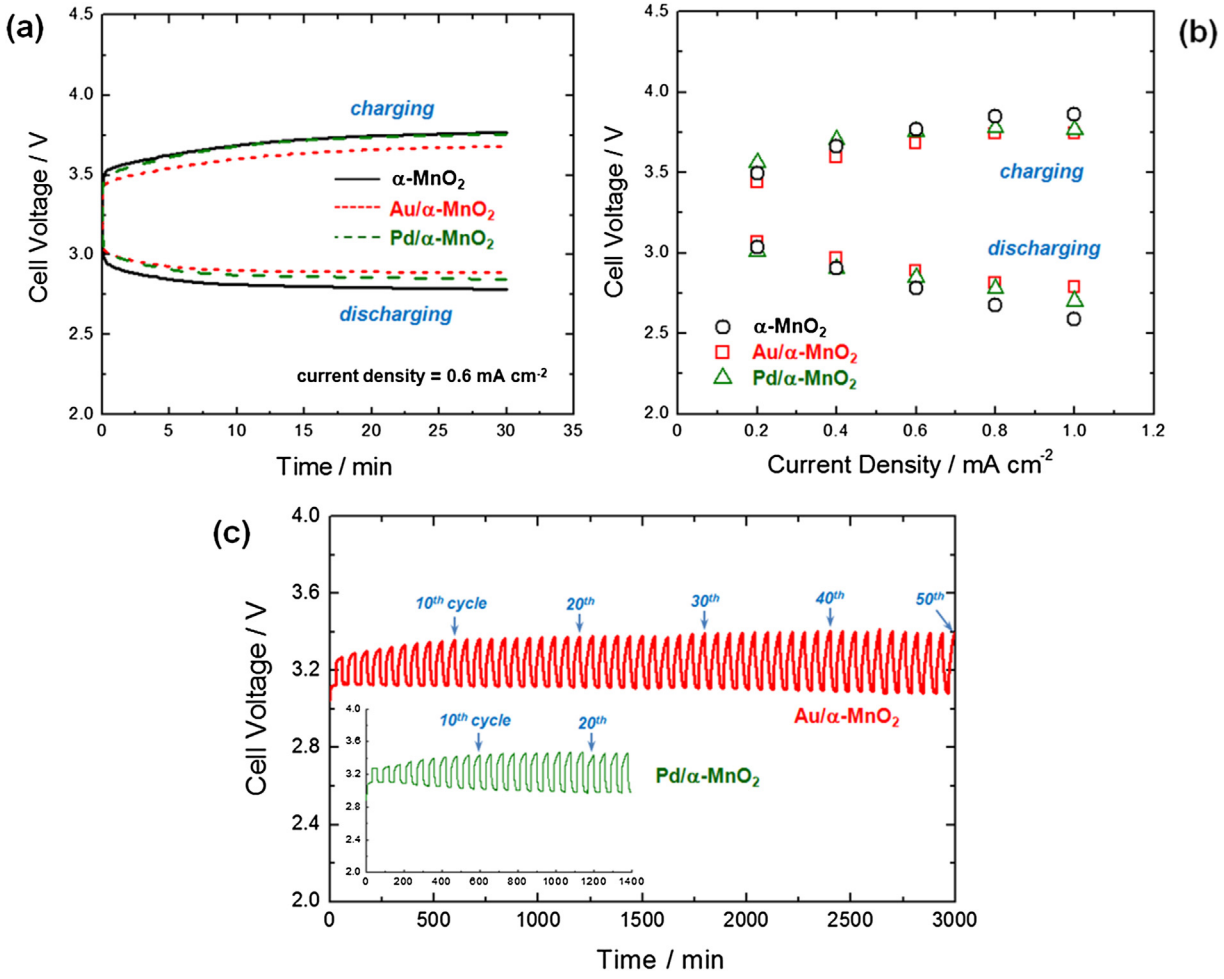

Fig. 7. (a) Discharge and charge profiles of the hybrid Li–O_2 batteries with the pristine α-MnO_2, Au/α-MnO_2 and Pd/α-MnO_2 catalysts at a current density of 0.6 mA cm^{-2} and (b) the voltage *vs.* applied current plots. (c) Cycling performances measured using the Au/α-MnO_2 and Pd/α-MnO_2 catalysts.

membrane. Further analysis is in progress to determine the physical origins of the performance degradation using various characterization techniques.

4. Conclusion

Urchin-like α-MnO_2 materials decorated with Au and Pd nanoparticles were synthesized as a cathode catalyst for rechargeable hybrid Li–O_2 batteries. Au and Pd particles as large as 3–8 nm were successfully loaded on the vertically aligned nanorods of α-MnO_2. The electrochemical studies using the RDE and hybrid Li–O_2 batteries indicated that the Au/α-MnO_2 and Au/α-MnO_2 catalysts showed high bi-functional activity for both ORR and OER, leading to reduced discharge–charge overpotentials of the hybrid Li–O_2 battery. This study suggests that the metal-decorated α-MnO_2 can be used as an efficient bi-functional catalyst for rechargeable hybrid Li–O_2 batteries.

Acknowledgments

This work was supported by the Energy Efficiency & Resources of the Korea Institute of Energy Technology Evaluation and Planning (No. 20112020100110) grant funded by the Korea government Ministry of Knowledge Economy.

References

[1] F. Cheng, J. Chen, Chem. Soc. Rev. 41 (2012) 2172–2192.
[2] G. Girishkumar, B. McCloskey, A.C. Luntz, S. Swanson, W. Wilcke, J. Phys. Chem. Lett. 1 (2010) 2193–2203.
[3] J. Christensen, P. Albertus, R.S. Sanchez-Carrera, T. Lohmann, B. Kozinsky, R. Liedtke, J. Ahmed, A. Kojic, J. Electrochem. Soc. 159 (2012) R1–R30.
[4] E.L. Littauer, K.C. Tsai, J. Electrochem. Soc. 123 (1976) 771–776.
[5] K.M. Abraham, Z. Jiang, J. Electrochem. Soc. 143 (1996) 1–5.
[6] A. Débart, J. Bao, G. Armstrong, P.G. Bruce, J. Power Sources 174 (2007) 1177–1182.
[7] A. Débart, A.J. Paterson, J. Bao, P.G. Bruce, Angew. Chem. Int. Ed. 120 (2008) 4597–4600.
[8] Y.C. Lu, Z. Xu, H.A. Gasteiger, S. Chen, K. Hamad-Schifferli, Y. Shao-Horn, J. Am. Chem. Soc. 132 (2010) 12170–12171.
[9] Y. Shao, S. Park, J. Xiao, J.G. Zhang, Y. Wang, J. Liu, ACS Catal. 2 (2012) 844–857.
[10] S.A. Freunberger, Y. Chen, Z. Peng, J.M. Griffin, L.J. Hardwick, F. Bardé, P. Novák, P.G. Bruce, J. Am. Chem. Soc. 133 (2011) 8040–8047.
[11] B.D. McCloskey, D.S. Bethune, R.M. Shelby, G. Girishkumar, A.C. Luntz, J. Phys. Chem. Lett. 2 (2011) 1161–1166.
[12] Y. Wang, H. Zhou, J. Power Sources 195 (2010) 358–361.
[13] H. Zhou, Y. Wang, H. Li, P. He, ChemSusChem 3 (2010) 1009–1019.
[14] E. Yoo, H. Zhou, ACS Nano 5 (2011) 3020–3026.
[15] L. Wang, X. Zhao, Y. Lu, M. Xu, D. Zhang, R.S. Ruoff, K.J. Stevenson, J.B. Goodenough, J. Electrochem. Soc. 158 (2011) A1379–A1382.
[16] H. Wang, Y. Yang, Y. Liang, G. Zheng, Y. Li, Y. Cui, H. Dai, Energy Environ. Sci. 5 (2012) 7931–7935.
[17] I. Arul Raj, K.I. Vasu, Int. J. Hydrogen Energy 15 (1990) 751–756.
[18] F.H.B. Lima, M.L. Calegaro, E.A. Ticianelli, J. Electrochem. Soc. 590 (2006) 152–160.

[19] F. Cheng, Y. Su, J. Liang, Z. Tao, J. Chen, Chem. Mater. 22 (2010) 898–905.
[20] V. Neburchilov, H. Wang, J.J. Martin, W. Qu, J. Power Sources 195 (2010) 1271–1291.
[21] M.M. Thackeray, Prog. Solid State Chem. 25 (1997) 1–71.
[22] T.J. Schmidt, V. Stamenkovic, M. Arenz, N.M. Markovic, P.N. Ross, Electrochim. Acta 47 (2002) 3765–3776.
[23] L. Jiang, A. Hsu, D. Chu, R. Chen, J. Electrochem. Soc. 156 (2009) B370–B376.
[24] Y. Lee, A. Loew, S. Sun, Chem. Mater. 22 (2010) 755–761.
[25] X. Li, B.N. Popov, T. Kawahara, H. Yanagi, J. Power Sources 196 (2011) 1717–1722.
[26] S. Treimer, A. Tang, D.C. Johnson, Electroanalysis 14 (2002) 165–171.
[27] E.M. Benbow, S.P. Kelly, L. Zhao, J.W. Reutenauer, S.L. Suib, J. Phys. Chem. C 115 (2011) 22009–22017.
[28] W. Tang, H. Lin, A. Kleiman-Shwarsctein, G.D. Stucky, E.W. McFarland, J. Phys. Chem. C 112 (2008) 10515–10519.
[29] L. Jiang, A. Hsu, D. Chu, R. Chen, J. Electrochem. Soc. 156 (2009) B643–B649.